arXiv:1512.06909v1 [hep-ph] 21 Dec 2015

The quark susceptibility in a generalized dynamical quasiparticle model

H. Berrehrah,[1,2,*] W. Cassing,[3,†] E. Bratkovskaya,[1,2,‡] and Th. Steinert[3,§]

[1] *Frankfurt Institute for Advanced Studies, Johann Wolfgang Goethe Universität, Ruth-Moufang-Strasse 1, 60438 Frankfurt am Main, Germany*
[2] *Institut for Theoretical Physics, Johann Wolfgang Goethe Universität, Max-von-Laue-Str. 1, 60438 Frankfurt am Main, Germany*
[3] *Institut für Theoretische Physik, Universität Giessen, 35392 Giessen, Germany*

The quark susceptibility χ_q at zero and finite quark chemical potential provides a critical benchmark to determine the quark-gluon-plasma (QGP) degrees of freedom in relation to the results from lattice QCD (lQCD) in addition to the equation of state and transport coefficients. Here we extend the familiar dynamical-quasiparticle model (DQPM) to partonic propagators that explicitly depend on the three-momentum with respect to the partonic medium at rest in order to match perturbative QCD (pQCD) at high momenta. Within the extended dynamical-quasi-particle model (DQPM*) we reproduce simultaneously the lQCD results for the quark number density and susceptibility and the QGP pressure at zero and finite (but small) chemical potential μ_q. The shear viscosity η and the electric conductivity σ_e from the extended quasiparticle model (DQPM*) also turn out in close agreement with lattice results for μ_q =0. The DQPM*, furthermore, allows to evaluate the momentum p, temperature T and chemical potential μ_q dependencies of the partonic degrees of freedom also for larger μ_q which are mandatory for transport studies of heavy-ion collisions in the regime 5 GeV $< \sqrt{s_{NN}} <$ 10 GeV.

PACS numbers: 24.10.Jv, 02.70.Ns, 12.38.Mh, 24.85.+p

I. INTRODUCTION

The thermodynamic properties of the quark-gluon plasma (QGP)–as produced in relativistic heavy-ion collisions–is well determined within lattice QCD (lQCD) calculations at vanishing quark chemical potential [1–6]. At non-zero quark chemical potential $\mu_q \neq 0$, the primary quantities of interest are the "pressure difference ΔP", the quark number density n_B and quark susceptibility χ_q since these quantities are available from lQCD [7, 8]. The lQCD results can conveniently be interpreted within quasiparticle models [9–16] that are fitted to the equation of state from lQCD and also allow for extrapolations to finite μ_q, although with some ambiguities. The quark number susceptibilities are additional quantities to further quantify the properties of the partonic degrees of freedom (d.o.f.) especially in the vicinity of the QCD phase transition or crossover [4, 5, 17].

Some early attempts to describe the lQCD pressure were based on the notion of the QGP as a free gas of massless quarks and gluons [18] (Stephan-Boltzmann limit), or on the assumption of interacting massless quarks and gluons following perturbative QCD interactions [19], or even as perturbative thermal massive light quarks and gluons in the Hard-Thermal-Loop (HTL) approximation [20]. These attempts failed to reproduce lQCD results especially in the region 1 – 3 T_c. Some phenomenological models, based on the notion of the QGP as weakly interacting quasi-particels (QPM) have been constructed to reproduce the pressure and entropy from lQCD [15, 21]. Nevertheless, the challenge of describing simultaneously both the lQCD pressure and quark susceptibilities as well as transport coefficients is out of reach in these models [15], especially if the quasi-particle model is not fitted to quark susceptibilities but to the entropy density as common to most approaches. Such findings have been pointed out before in Ref. [16] where the QPM underestimates the data on susceptibilities since lattice results already reach the ideal gas limit for temperatures slightly above T_c, leaving little space for thermal parton masses. The apparent inconsistency between the description of QCD thermodynamics and susceptibilities within the standard quasi-particle model has been pointed out in particular in Refs. [15, 16]. Especially the quark susceptibilities are very sensitive to the quark masses that are used as inputs and solely determined by the quark degrees of freedom. On the other hand both light quark and gluon masses contribute to thermodynamic quantities like the entropy density and pressure. Therefore, reconciling all observables from lQCD within a single effective model is a challenge.

In this study we will consider the QGP as a dynamical quasi-particle medium of massive off-shell particles (as described by the dynamical quasiparticle model "DQPM" [22–24]) and extend the DQPM to partonic propagators that explicitly depend on the three-momentum with respect to the partonic matter at rest in order to match perturbative QCD (pQCD) at high momenta. We show that within the extended DQPM – denoted by DQPM* – we reproduce the lQCD equation of state at finite temperature T and chemical potential μ_q. Moreover, we simultaneously describe the quark number density and susceptibility χ_q from lQCD. In the same approach, we also compute the shear viscosity (η) and electric conductivity (σ_e) of the QGP at finite temperature

* berrehrah@fias.uni-frankfurt.de
† wolfgang.cassing@theo.physik.uni-giessen.de
‡ brat@th.physik.uni-frankfurt.de
§ thorsten.steinert@theo.physik.uni-giessen.de

and chemical potential in order to probe some transport properties of the partonic medium in analogy to the earlier studies in Refs. [25–28]. The partonic spectral functions (or imaginary parts of the retarded propagators) at finite temperature and chemical potential are determined for these dynamical quasi-particles and the shear viscosity η is computed within the relaxation-time approximation (RTA) which provides similar results as the Green-Kubo method employed in Refs. [29–31].

The paper is organized as follows: We first present in Section II the basic ingredients of the QGP d.o.f in terms of their masses and widths which are the essential ingredients in their retarded propagators as well as the running coupling (squared) $g^2(T,\mu_q,p)$. The gluon and fermion propagators – as given by the DQPM at finite momentum p, temperature T and quark chemical potential μ_q – contain a few parameters that have to be fixed in comparison to results from lQCD. The analysis of the lQCD pressure and interaction measure in a partonic medium at finite T and μ_q is performed in Section III while in Section IV we investigate the quark number density and susceptibility within the DQPM* and compare to lQCD results for 2+1 flavors ($N_f = 3$). In Section V we compute the QGP shear viscosity and compare to lQCD results and other theoretical studies while in Section VI we evaluate the electric conductivity of the QGP. Throughout Sections III-VI we will point out the importance of finite masses and widths of the dynamical quasiparticles, including their finite momentum, temperature and μ_q dependencies. In Section VII we summarize the main results and point out the future applications of the DQPM*.

II. PARTON PROPERTIES IN THE DQPM*

In the DQPM* the entropy density $s(T)$, the pressure $P(T)$ and energy density $\varepsilon(T)$ are calculated in a straight forward manner by starting with the entropy density in the quasiparticle limit from Baym [22, 32, 33],

$$\begin{aligned} s^{dqp} = &-d_g \int \frac{d\omega}{2\pi}\frac{d^3p}{(2\pi)^3}\frac{\partial n_B}{\partial T}\left(\Im \ln(-\Delta^{-1}) + \Im\Pi\,\Re\Delta\right) \\ &- d_q \int \frac{d\omega}{2\pi}\frac{d^3p}{(2\pi)^3}\frac{\partial n_F((\omega-\mu_q)/T)}{\partial T}\left(\Im \ln(-S_q^{-1}) + \Im\Sigma_q\,\Re S_q\right) \\ &- d_{\bar q} \int \frac{d\omega}{2\pi}\frac{d^3p}{(2\pi)^3}\frac{\partial n_F((\omega+\mu_q)/T)}{\partial T}\left(\Im \ln(-S_{\bar q}^{-1}) + \Im\Sigma_{\bar q}\,\Re S_{\bar q}\right), \end{aligned} \tag{II.1}$$

where $n_B(\omega/T) = (\exp(\omega/T)-1)^{-1}$ and $n_F((\omega-\mu_q)/T) = (\exp((\omega-\mu_q)/T)+1)^{-1}$ denote the Bose and Fermi distribution functions, respectively, while $\Delta = (P^2-\Pi)^{-1}$, $S_q = (P^2-\Sigma_q)^{-1}$ and $S_{\bar q} = (P^2-\Sigma_{\bar q})^{-1}$ stand for the full (scalar) quasiparticle propagators of gluons g, quarks q and antiquarks $\bar q$. In Eq. (II.1) Π and $\Sigma = \Sigma_q \approx \Sigma_{\bar q}$ denote the (retarded) quasiparticle selfenergies. In principle, Π as well as Δ are Lorentz tensors and should be evaluated in a nonperturbative framework. The DQPM treats these degrees of freedom as independent scalar fields with scalar selfenergies which are assumed to be identical for quarks and antiquarks. Note that one has to treat quarks and antiquarks separately in Eq. (II.1) as their abundance differs at finite quark chemical potential μ_q. In Eq. (II.1) the degeneracy for gluons is $d_g = 2(N_c^2-1)$=16 while $d_q = d_{\bar q}$=$2N_cN_f$=18 is the degeneracy for quarks and antiquarks with three flavors. As a next step one writes the complex selfenergies as $\Pi(\boldsymbol{q}) = M_g^2(\boldsymbol{q}) - 2i\omega\gamma_g(\boldsymbol{q})$ and $\Sigma_q(\boldsymbol{q}) = M_q(\boldsymbol{q})^2 - 2i\omega\gamma_q(\boldsymbol{q})$ with a mass (squared) term M^2 and an interaction width γ, i.e. the inverse retarded propagators (Δ, S_q) read,

$$G_R^{-1} = \omega^2 - \boldsymbol{q}^2 - M^2(\boldsymbol{q}) + 2i\gamma(\boldsymbol{q})\omega \tag{II.2}$$

and are analytic in the upper half plane in the energy ω. The imaginary part of (II.2) then gives the spectral function of the degree of freedom (except for a factor $1/\pi$). In the DQPM [22–24] the masses have been fixed in the spirit of the hard thermal loop (HTL) approach with the masses being proportional to an effective coupling $g(T/T_c)$ which has been enhanced in the infrared. In the DQPM* the selfenergies depend additionally on the three-momentum $(\boldsymbol{p})$ with respect to the medium at rest, while the dependence on the temperature T/T_c and chemical potential μ_q are very similar to the standard DQPM.

A. Masses, widths and spectral functions of partonic degrees of freedom in DQPM*

The functional forms for the partons masses and widths at finite temperature T, quark chemical potential μ_q and momentum p are assumed to be given by

$$M_g(T,\mu_q,p) = \left(\frac{3}{2}\right) \times \left[\frac{g^2(T^\star/T_c(\mu_q))}{6}\left[(N_c+\frac{1}{2}N_f)T^2+\frac{N_c}{2}\sum_q\frac{\mu_q^2}{\pi^2}\right]\times\left[\frac{1}{1+\Lambda_g(T_c(\mu_q)/T^\star)p^2}\right]\right]^{1/2}+m_{\chi g}\,,$$

$$M_{q,\bar{q}}(T,\mu_q,p) = \left[\frac{N_c^2-1}{8N_c}\,g^2(T^\star/T_c(\mu_q))\left[T^2+\frac{\mu_q^2}{\pi^2}\right]\times\left[\frac{1}{1+\Lambda_q(T_c(\mu_q)/T^\star)p^2}\right]\right]^{1/2}+m_{\chi q}\,,$$

$$\gamma_g(T,\mu_q,p) = N_c\,\frac{g^2(T^\star/T_c(\mu_q))}{8\pi}\;T\,\ln\left(\frac{2c}{g^2(T^\star/T_c(\mu_q))}+1.1\right)^{3/4}\times\left[\frac{1}{1+\Lambda_g(T_c(\mu_q)/T^\star)p^2}\right]^{1/2},$$

$$\gamma_{q,\bar{q}}(T,\mu_q,p) = \frac{N_c^2-1}{2N_c}\,\frac{g^2(T^\star/T_c(\mu_q))}{8\pi}\,T\ln\left(\frac{2c}{g^2(T^\star/T_c(\mu_q))}+1.1\right)^{3/4}\times\left[\frac{1}{1+\Lambda_q(T_c(\mu_q)/T^\star)p^2}\right]^{1/2}, \tag{II.3}$$

where $T^{\star 2}=T^2+\mu_q^2/\pi^2$ is the effective temperature used to extend the DQPM to finite μ_q, $\Lambda_g(T_c(\mu_q)/T^\star)=5\;\;(T_c(\mu_q)/T^\star)^2$ GeV^{-2} and $\Lambda_q(T_c(\mu_q)/T^\star)=12\;\;(T_c(\mu_q)/T^\star)^2$ GeV^{-2}. Here $m_{\chi g}\approx 0.5$ GeV is the gluon condensate and $m_{\chi q}$ is the light quark chiral mass ($m_{\chi q}=0.003$ GeV for u, d quarks and $m_{\chi q}=0.06$ GeV for s quarks). In Eq. (II.3) $m_{\chi g}$ ($m_{\chi q}$) gives the finite gluon (light quark) mass in the limit $p\to 0$ and $T=0$ or for $p\to\infty$. As mentioned above the quasiparticle masses and widths (II.3) are parametrized following hard thermal loop (HTL) functional dependencies at finite temperature as in the default DQPM [22] in order to follow the correct high temperature limit. The essentially new elements in (II.3) are the multiplicative factors specifying the momentum dependence of the masses and widths with additional parameters Λ_g and Λ_q and the additive terms $m_{\chi g}$ and $m_{\chi q}$. The momentum-dependent factor in the masses (II.3) is motivated by Dyson-Schwinger studies in the vacuum [34] and yields the limit of pQCD for $p\to\infty$.

The effective gluon and quark masses are a function of $T^\star$ at finite μ_q. Here we consider three light flavors ($q=u,d,s$) and assume all chemical potentials to be equal ($\mu_u=\mu_d=\mu_s=\mu_q$). Note that alternative settings are also possible to comply with strangeness neutrality in heavy-ion collisions. The coupling (squared) g^2 in (II.3) is the effective running coupling given as a function of T/T_c at $\mu_q=0$. A straight forward extension of the DQPM to finite μ_q is to consider the coupling as a function of $T^\star/T_c(\mu_q)$ with a μ_q-dependent critical temperature $T_c(\mu_q)$,

$$T_c(\mu_q) = T_c(\mu_q=0)\sqrt{1-\alpha\mu_q^2}\approx T_c(\mu_q=0)\left(1-\alpha/2\mu_q^2+\ldots\right) \tag{II.4}$$

with $\alpha\approx 8.79$ GeV^{-2}. We recall that the expression of $T_c(\mu_q)$ in (II.4) is obtained by requiring a constant energy density ε for the system at $T=T_c(\mu_q)$ where ε at $T_c(\mu_q=0)\approx 0.158$ GeV is fixed by lattice QCD calculation at $\mu_q=0$. The coefficient in front of the μ_q^2-dependent part can be compared to lQCD calculations at finite (but small) μ_B which gives [35]

$$T_c(\mu_B) = T_c(\mu_B=0)\left(1-\kappa\left(\frac{\mu_B}{T_c(\mu_B=0)}\right)^2+\ldots\right) \tag{II.5}$$

with $\kappa=0.013(2)$. Rewriting (II.4) in the form (II.5) and using $\mu_B\approx 3\mu_q$ we get $\kappa_{DQPM}\approx 0.0122$ which compares very well with the lQCD result.

Using the pole masses and widths (II.3), the spectral functions for the partonic degrees of freedom are fully determined, i.e. the imaginary parts of the retarded propagators. The real part of the retarded propagators then follows from dispersion relations. Since the retarded propagators show no poles in the upper complex half plane in the energy ω the model propagators obey micro-causality [36]. The imaginary parts are of Lorentzian form and provide the spectral functions $\rho_i(p)$ with $p=(\omega,\boldsymbol{p})$ [22, 37, 38],

$$\rho_i(\omega,\boldsymbol{p}) = \frac{4\omega\gamma_i(\boldsymbol{p})}{(\omega^2-\boldsymbol{p}^2-M_i^2(\boldsymbol{p}))^2+4\gamma_i^2(\boldsymbol{p})\omega^2} \equiv \frac{\gamma_i(\boldsymbol{p})}{\tilde{E}_i(\boldsymbol{p})}\left(\frac{1}{(\omega-\tilde{E}_i(\boldsymbol{p}))^2+\gamma_i^2(\boldsymbol{p})}-\frac{1}{(\omega+\tilde{E}_i(\boldsymbol{p}))^2+\gamma_i^2(\boldsymbol{p})}\right) \tag{II.6}$$

with $\tilde{E}_i^2(\boldsymbol{p})=\boldsymbol{p}^2+M_i^2(\boldsymbol{p})-\gamma_i^2(\boldsymbol{p})$ for $i\in[g,q,\bar{q}]$. These spectral functions (II.6) are antisymmetric in ω and normalized as

$$\int_{-\infty}^{+\infty}\frac{d\omega}{2\pi}\;\omega\;\rho_i(\omega,\boldsymbol{p}) = \int_0^{+\infty}\frac{d\omega}{2\pi}\;2\omega\;\rho_i(\omega,\boldsymbol{p}) = 1. \tag{II.7}$$

where $M_i(T,\mu_q,\boldsymbol{p})$, $\gamma_i(T,\mu_q,\boldsymbol{p})$ are the particle pole mass and width at finite three momentum $\boldsymbol{p}$, temperature T and chemical potential μ_q, respectively.

B. The running coupling in DQPM*

In contrast to our previous DQPM studies in Refs. [26–28] we suggest here a new solution for the determination of the effective coupling which is more flexible. Our new strategy to determine $g^2(T(T_c)$ is the following: For every temperature T we fit the DQPM* entropy density (II.1) to the entropy density s^{lQCD} obtained by lQCD. In practice, it has been checked that for a given value of g^2, the ratio $s(T,g^2)/T^3$ is almost constant for different temperatures and identical to g^2. Moreover $\frac{\partial}{\partial T}(s(T,g^2)/T^3)=0$. Therefore the entropy density s and the dimensionless equation of state in the DQPM* is a function of the effective coupling only, i.e. $s(T,g^2)/s_{SB}(T)=f(g^2)$. The functional form

$$f(g^2)=\frac{1}{(1+a_1.(g^2)^{a_2})^{a_3}}$$

is suited to describe $s^{lQCD}(T,g^2)/s_{SB}$. By inverting $f(g^2)$, one arrives at the following parametrization for g^2 as a function of s/s_{SB}:

$$g^2(s/s_{SB},T)\sim\left(\frac{a}{T}+b\right)\left(\left(\frac{s/s_{SB}}{d(T)}\right)^{v(T)}-1\right)^{w(T)}, \tag{II.8}$$

with $S_{SB}^{QCD}=19/(9\pi^2T^3)$. Since the entropy density from lQCD has the proper high temperature limit, the effective coupling g^2 also gives the correct asymptotics for $T\to\infty$ and decreases as $g^2\sim 1/\log(T^2)$. The temperature-dependent parameters $v(T)$, $w(T)$ and $d(T)$ all have the functional form:

$$f(T)=\frac{a}{(T^b+c)^d}.(T+e), \tag{II.9}$$

where the parameters a, b, c, d and e are fixed once for each function $v(T)$, $w(T)$ and $d(T)$.

Note that with the parametrization (II.8) for $g^2(s/s_{SB},T)$ one can easily adapt to any equation of state and therefore avoid a refitting of the coupling in case of new (or improved) lattice data. However, the coupling (II.8) is valid only for a given number of quark flavors N_f which is fixed by the lQCD equation of state.

To obtain $g^2(T/T_c)$ from $g^2(s/s_{SB},T)$, we proceed as follows:

- Using the equation of state from the Wuppertal-Budapest collaboration [7], which provide an analytical parametrization of the interaction measure I/T^4,

$$\frac{I(T)}{T^4}=\exp(-h_1/t-h_2/t^2).\left(h_0+\frac{f_0(\tanh(f_1.t+f_2)+1)}{1+g_1.t+g_2.t^2}\right), \tag{II.10}$$

  with $t=T/200$ MeV, $h_0=0.1396$, $h_1=-0.18$, $h_2=0.035$, $f_0=2.76$, $f_1=6.79$, $f_2=-5.29$, $g_1=-0.47$ and $g_2=1.04$,

- we calculate the pressure P/T^4 by

$$\frac{P(T)}{T^4}=\int_0^T\frac{I(T_0)}{T_0^5}dT_0, \tag{II.11}$$

- and then the entropy density s/s_{SB}

$$s/s_{SB}=\frac{I(T)/T^4+4P/T^4}{19/(9\pi^2)}. \tag{II.12}$$

- Replacing s/s_{SB} from Eq.(II.12) in Eq.(II.8) we obtain $g^2(T/T_c)$.

The procedure outlined above yields $g^2(T/T_c)$ for $\mu_q=0$. For finite μ_q we will make use of $g^2(T/T_c)\to g^2(T^\star/T_c(\mu_q))$, with the μ_q-dependent critical temperature $T_c(\mu_q)$ taken from (II.4). The running coupling (II.8)-(II.12) permits for an enhancement near T_c as already introduced in Ref. [12].

Figs. 1, (a)-(b) show the gluon and light quark masses and widths, respectively, at finite temperature and chemical potential for a momentum $p=1$ GeV/c. Furthermore, Fig. 1 (c) shows the gluon and light quark masses as a function of momentum (squared) p^2 at finite temperature $T=2T_c$ and different μ_q. Note that for $p=0$ we obtain higher values of the gluon and light quark masses (as a function of T and μ_q) since for finite momenta the masses decrease (at a given temperature and chemical potential), especially for the light quarks as seen in Fig 1 (c). The extension $T/T_c\to T^\star/T_c(\mu_q)$ for finite μ_q in the functional form for the strong coupling leads to lower values for the parton masses and widths at finite μ_q as compared to $\mu_q=0$ near $T_c(\mu_q)$.

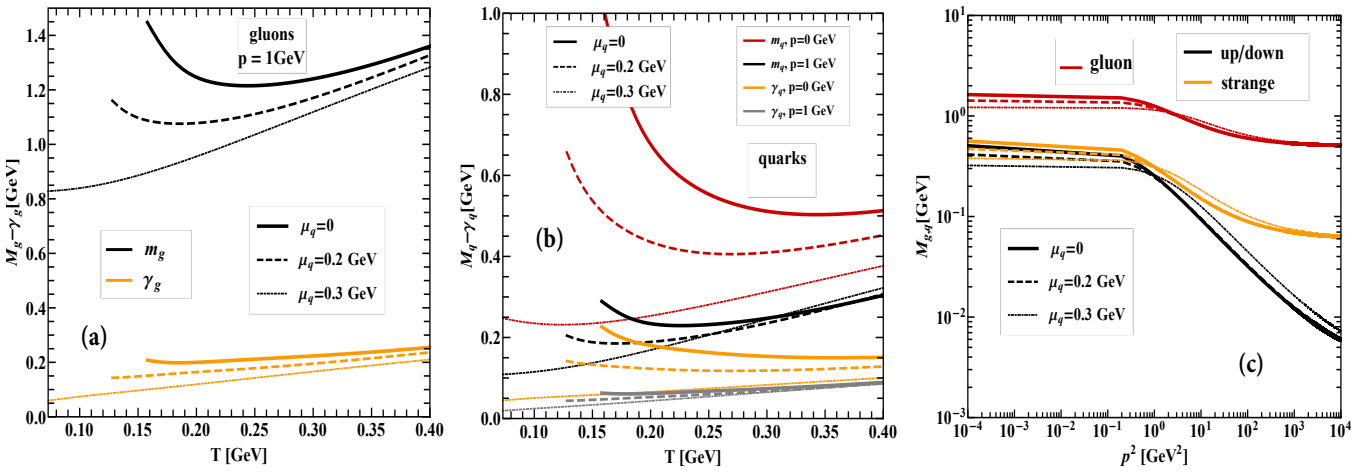

FIG. 1. *(Color online) The DQPM* gluon (a) and light quark (b) masses and widths given by (II.3) using the coupling (II.8)-(II.12) for different quark chemical potentials as a function of the temperature T. (c) Gluon and light quark masses as a function of the momentum squared for $T = 2T_c$ and $\mu_q = 0, 0.2, 0.3$ GeV.*

III. THERMODYNAMICS OF THE QGP FROM DQPM*

The expressions for the equation of state (energy density ε, entropy density s and pressure P) of strongly interacting matter have been given for finite temperature and chemical potential in Ref. [39] for on-shell partons and in [22] for the case of off-shell partons using the relations based on the stress-energy tensor $T^{\mu\nu}$. We recall that the approach for calculating the equation of state in the DQPM* is based on thermodynamic relations (see below). The procedure is as follows: One starts from the evaluation of the entropy density s from (II.1) employing the masses and widths obtained from the expressions (II.1). Then using the thermodynamic relation $s = (\partial P/\partial T)_{\mu_q}$ (for a fixed quark chemical potential μ_q) one obtains the pressure P by integration of s over T while the energy density ε can be gained using the relation,

$$Ts(T,\mu_B) = \varepsilon(T,\mu_B) + P(T,\mu_B) - \mu_B n_B(T,\mu_B), \tag{III.1}$$

where n_B is the net baryon density.

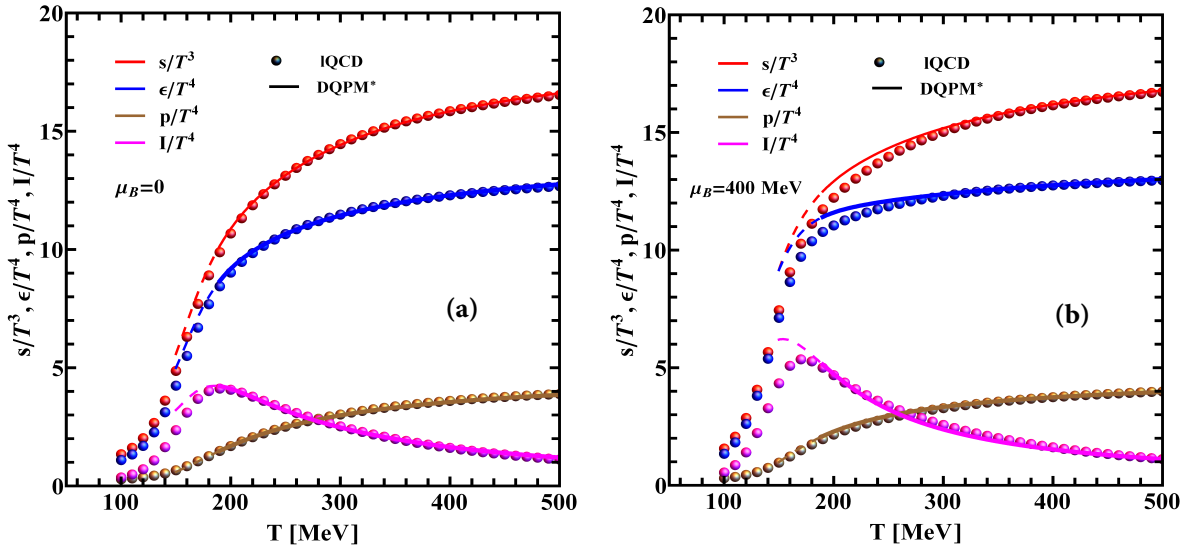

FIG. 2. *(Color online) Energy density ε, entropy density s, pressure density P and trace anomaly $(I = \varepsilon - 3P)$ as a function of temperature T at $\mu_B = 0$ (a) and at $\mu_B = 400$ MeV (b) from DQPM* compared to lQCD data from Ref. [7].*

The energy density ε, entropy density s, pressure P and the interaction measure $[I(T,\mu_q) = \varepsilon(T,\mu_q) - 3P(T,\mu_q)]$ –known in lQCD as the trace anomaly– in the DQPM* are shown in Fig.2 (a), (b) as a function of temperature T for two values of the baryon

chemical potential $\mu_B = 0$ and $\mu_B = 400$ MeV, respectively (where $\mu_B = 3\mu_q$ in our study). We, furthermore, compare our results with lattice calculations from Ref. [7]. We notice that our results are in a very good agreement with the lattice data for $\mu_B = 0$ (a) and in case of $\mu_B = 400$ MeV (b) for temperatures larger than 1.2 $T_c(\mu_q)$. In the latter case we observe (for temperatures just above $T_c(\mu)$) some deviations which are expected to result from additional hadronic degrees of freedom in the crossover region. The excess in quarks can be seen also in the net baryon density n_B, as we will show below.

At finite baryon chemical potential i.e. $\mu_B = 400$ MeV, the maximum of the trace anomaly is shifted towards lower temperatures. We notice also the proper scaling of our DQPM* description of QGP thermodynamics, when moving from zero to finite quark chemical potential (cf. Fig.2 (a) and (b)).

IV. QUARK NUMBER DENSITY AND SUSCEPTIBILITY FROM DQPM*

A. Baryon number density in the DQPM*

The equation of state for vanishing chemical potential is defined solely by the entropy density; for finite chemical potential one has to include the particle density. In the DQPM* the quark density n^{dqp} in the quasiparticle limit is defined in analogy to the entropy density (II.1) as [40],

$$\begin{aligned} n^{dqp} = &-d_q \int \frac{d\omega}{2\pi} \frac{d^3p}{(2\pi)^3} \frac{\partial n_F((\omega-\mu_q)/T)}{\partial \mu_q} \left(\Im \ln(-S_q^{-1}) + \Im\Sigma_q \, \Re S_q\right) \\ &- d_{\bar q} \int \frac{d\omega}{2\pi} \frac{d^3p}{(2\pi)^3} \frac{\partial n_F((\omega+\mu_q)/T)}{\partial \mu_q} \left(\Im \ln(-S_{\bar q}^{-1}) + \Im\Sigma_{\bar q} \, \Re S_{\bar q}\right), \end{aligned} \tag{IV.1}$$

and n_B from (IV.1) is split following the on-shell $n_B^{(0)}$ and off-shell Δn_B terms, with $n_B = n_B^{(0)} + \Delta n_B$ as:

$$n_B^{(0)} = d_q \int \frac{d^3p}{(2\pi)^3} \, f_q^{(0)} - d_{\bar q} \int \frac{d^3p}{(2\pi)^3} \, f_{\bar q}^{(0)}, \tag{IV.2}$$

$$\begin{aligned} \Delta n_B = &\int \frac{d\omega}{(2\pi)} \frac{d^3p}{(2\pi)^3} \frac{\partial f_q((\omega-\mu_q)/T)}{\partial \mu_q} \left(2\gamma\omega \frac{\omega^2 - \mathbf{p}^2 - M^2}{(\omega^2 - \mathbf{p}^2 - M^2)^2 + 4\gamma^2\omega^2} - \arctan\left(\frac{2\gamma\omega}{\omega^2 - \mathbf{p}^2 - M^2}\right)\right) \\ &+ \int \frac{d\omega}{(2\pi)} \frac{d^3p}{(2\pi)^3} \frac{\partial f_{\bar q}((\omega+\mu_q)/T)}{\partial \mu_q} \left(2\gamma\omega \frac{\omega^2 - \mathbf{p}^2 - M^2}{(\omega^2 - \mathbf{p}^2 - M^2)^2 + 4\gamma^2\omega^2} - \arctan\left(\frac{2\gamma\omega}{\omega^2 - \mathbf{p}^2 - M^2}\right)\right), \end{aligned} \tag{IV.3}$$

where $f_q^{(0)} = (\exp((\sqrt{p^2+M^2} - \mu_q)/T) + 1)^{-1}$, $f_{\bar q}^{(0)} = (\exp((\sqrt{p^2+M^2} + \mu_q)/T) + 1)^{-1}$ denote again the Fermi distribution functions for the on-shell quark and anti-quark, with M corresponding to the pole mass. The on- and off-shell terms can be interpreted as arising from a pole- and a damping-term, respectively. The pole term $n_B^{(0)}$ corresponds to the baryon density of a non-interacting massive gas of quasiparticles, whereas the additional contribution due to the damping term Δn_B has to be attributed to the finite width of the quasiparticles.

Finally, note that the quark number density follows from the same potential as the entropy density [33] which ensures that it fulfills the thermodynamic relation $n = (\partial P/\partial \mu_q)_T$ (for fixed temperature T). To be fully thermodynamically consistent the entropy and the particle density have to satisfy the Maxwell relation $(\partial n/\partial T)_{\mu_q} = (\partial s/\partial \mu_q)_T$. This provides further constraints on the effective coupling $g^2(T,\mu_q)$ at finite chemical potential which we neglect in the current approach. Nevertheless, it was checked that the violation of the Maxwell relation is generally small and most pronounced around T_c. We note, however, that when extending the approach to even larger chemical potentials the full thermodynamic consistency has to be taken into account. The baryon number density, finally, is related to the quark number density by the simple relation $n_B = n^{dqp}/3$.

B. Susceptibilities in the DQPM*

From the densities n_B one may obtain other thermodynamic quantities like the pressure difference ΔP and the quark susceptibilities χ_q, which can be confronted with lattice data for $N_f = 2$ from Alton *et al.* [41, 42] and for $N_f = 3$ from Borsanyi *et al.*[7]. We recall that the quark-number susceptibility measures the static response of the quark number density to an infinitesimal variation of the quark chemical potential. From (IV.2)-(IV.3) we calculate ΔP and χ_q as

$$\Delta P(T,\mu_B) \equiv P(T,\mu_B) - P(T,0) = \int_0^{\mu_B} n_B \, d\mu_B. \tag{IV.4}$$

$$\chi_q(T) = \left.\frac{\partial n_q}{\partial \mu_q}\right|_{\mu_q=0}; \qquad \chi_q(T,\mu_q) = \frac{1}{9}\frac{\partial n_B}{\partial \mu_B}. \tag{IV.5}$$

Furthermore, for small μ_q a Taylor expansion of the pressure in μ_q/T can be performed which gives

$$\frac{P(T,\mu_q)}{T^4} = \sum_{n=0}^{\infty} c_n(T)\left(\frac{\mu_q}{T}\right)^n, \qquad c_n(T) = \frac{1}{n!}\left.\frac{\partial^n (P(T,\mu_q)/T^4)}{\partial(\mu_q/T)^n}\right|_{\mu_q=0}, \tag{IV.6}$$

where $c_n(T)$ is vanishing for odd n and $c_0(T)$ is given by $c_0(T) = p(T,\mu_q=0)$. As shown above the DQPM* compares well with lattice QCD results for $c_0(T)$. Since χ_q at finite μ_q is related to the pressure by

$$\chi_q(T,\mu_q)/T^2 = \partial^2(P/T^4)/\partial^2(\mu_q/T),$$

one can define the susceptibility χ_2^{ij} at vanishing quark chemical potential as [7]

$$\frac{P(T,\mu_i)}{T^4} = \frac{P(T,0)}{T^4} + \frac{1}{2}\sum_{i,j}\frac{\mu_i\mu_j}{T^2}\chi_2^{ij}, \qquad \text{with } \chi_2^{ij} = \frac{1}{T^2}\left.\frac{\partial n_j(T,\mu_i)}{\partial \mu_i}\right|_{\mu_i=\mu_j=0}, \tag{IV.7}$$

which in case of 3 flavors (u, d, s quarks) with $\mu_u = \mu_d = \mu_s$ becomes

$$\chi_2(T) = \frac{1}{9}\,\frac{1}{T^2}\left.\frac{\partial n_q(T,\mu_q)}{\partial \mu_q}\right|_{\mu_q=0} = \frac{1}{9}\,\frac{\chi_q(T)}{T^2}. \tag{IV.8}$$

We recall again that the susceptibilities are the central quantities in lQCD calculations for nonzero μ_q.

C. n_B and χ_q: DQPM* *vs* lQCD

Using the masses and widths (II.3) and the running coupling (II.8)-(II.11), we calculate the baryon number density n_B (IV.2)-(IV.3) and quark susceptibility χ_2 including the finite width of the parton spectral functions. The results for n_B and χ_2 for $N_f = 3$ are given in Fig.3 (a) and (b), respectively. The comparison with the lattice data from [7] is rather good which is essentially due to an extra contribution arising from the momentum dependence of the DQPM* quasiparticles masses and widths. Such a momentum dependence in $m_{q,\bar{q},g}$ and $\gamma_{q,\bar{q},g}$ decreases the 'thermal average' of light quark and gluon masses which improves the description of lQCD results for the susceptibilities. For comparison we also show the result for χ_q from the conventional DQPM, i.e. with momentum independent masses, which substantially underestimates the lattice data. The small difference between lQCD and DQPM* for n_B and χ_2 close to T_c is related to a possible excess of light quarks and antiquarks which should combine to hadrons in the crossover region. We recall that the DQPM* describes only the QGP phase and deals with dynamical quarks and gluons solely.

Finally, we emphasize the challenge to describe simultaneously the entropy s and pressure P on one side and n_B and χ_2 on the other side. Indeed, increasing the light quark mass and width helps to improve the description of s and P (for μ_B = 400 MeV), but this leads to a considerable decrease in n_B and χ_2. In other words, lighter quarks are favorable to improve the agreement with lQCD data on n_B and χ_2, however, this leads to an increase of s and P, which can be only partially counterbalanced by an increasing gluon mass and width.

V. SHEAR VISCOSITY OF THE QGP FROM DQPM*

In this Section we focus on the shear viscosity of the QGP using the relaxation time approximation (RTA). In the dilute gas approximation the relaxation time τ_i of the particle i is obtained for on- or off-shell quasi-particles by means of the partonic scattering cross sections, where the qq, $q\bar{q}$, qg and gg elastic scattering processes as well as some inelastic processes involving chemical equilibration, such as $gg \to q\bar{q}$ are included in the computation of τ_i [27]. For the DQPM* approach we do not need the explicit cross sections since the inherent quasi-particle width $\gamma_i(T,\mu_q,p)$ directly provides the total interaction rate [22]. To this end we only have to evaluate the average of the momentum dependent widths $\gamma_g(T,\mu_q,p)$ and $\gamma_q(T,\mu_q,p)$ over the thermal distributions at fixed T and μ_q, i.e. $\bar{\gamma}_g(T,\mu_q)$ and $\bar{\gamma}_q(T,\mu_q)$.

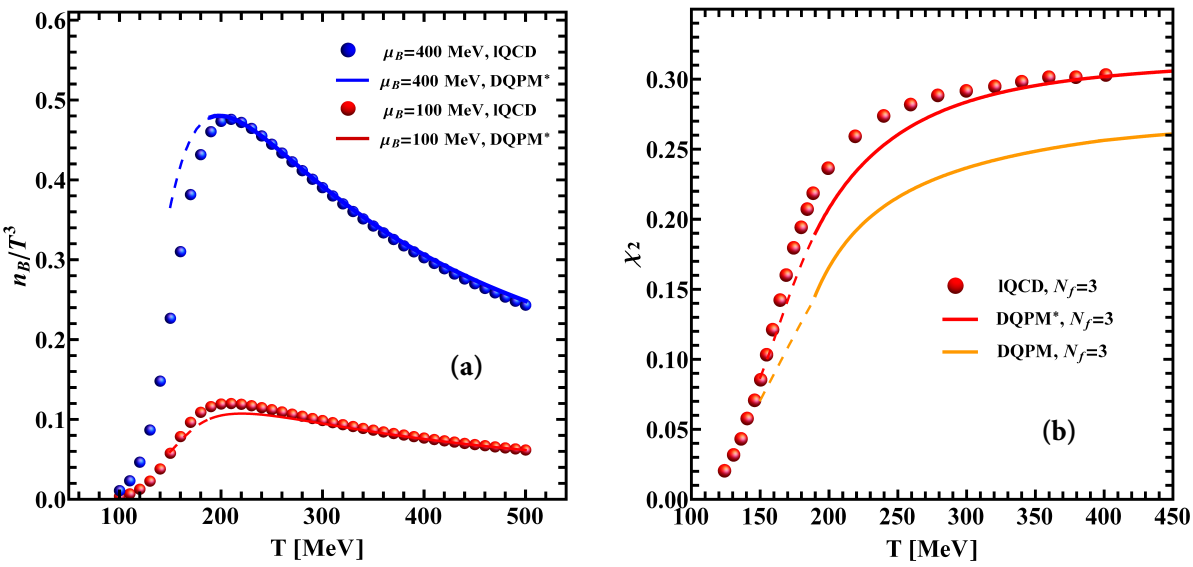

FIG. 3. *(Color online) (a) The baryon number density n_B from DQPM* as compared to lattice data from [7] for $N_f = 3$ for quark chemical potential $\mu_q = 0$. (b) The susceptibility χ_2 from DQPM* as compared to lattice data from [7] for $N_f = 3$ and $\mu_q = 0$ using Eq. (IV.8). The lower (orange) line gives the result from the conventional DQPM, i.e. with momentum independent masses.*

The shear viscosity $\eta(T,\mu_q)$ is defined in the dilute gas approximation for the case of off-shell particles by [27, 43]

$$\eta(T,\mu_q) = \frac{1}{15T} d_g \int \frac{d^3p}{(2\pi)^3} \int \frac{d\omega}{2\pi} \omega\ \bar{\tau}_g(T,\mu_q)\ f_g(\omega/T) \times \rho_g(\omega,\boldsymbol{p}) \frac{\boldsymbol{p}^4}{\omega^2} \Theta(P^2)$$
$$+ \frac{1}{15T} \frac{d_q}{6} \int \frac{d^3p}{(2\pi)^3} \int \frac{d\omega}{2\pi} \omega \left[\sum_q^{u,d,s} \bar{\tau}_q(T,\mu_q) f_q((\omega-\mu_q)/T) \rho_q(\omega,\boldsymbol{p}) + \sum_{\bar{q}}^{\bar{u},\bar{d},\bar{s}} \bar{\tau}_{\bar{q}}(T,\mu_q) f_{\bar{q}}((\omega+\mu_q)/T)\ \rho_{\bar{q}}(\omega,\boldsymbol{p}) \right] \frac{\boldsymbol{p}^4}{\omega^2} \Theta(P^2), \quad \text{(V.1)}$$

where $\boldsymbol{p}$ is the three-momentum and P^2 the invariant mass squared. The functions $\rho_g, \rho_q, \rho_{\bar{q}}$ stand for the gluon, quark and antiquark spectral functions, respectively, and f_q ($f_{\bar{q}}$) stand for the equilibrium distribution functions for particle and antiparticle. The medium-dependent relaxation times $\bar{\tau}_{q,g}(T,\mu_q)$ in (V.1) are given in the DQPM* by:

$$\bar{\tau}_{q,g}(T,\mu_q) = (\bar{\gamma}_{q,g})^{-1}(T,\mu_q), \quad \text{(V.2)}$$

with:

$$\bar{\gamma}_{q,g}(T,\mu_q) = \langle \gamma_{q,g}(T,\mu_q,p) \rangle_p = \left(n^{\rm off}_{q,g}(T,\mu_q)\right)^{-1} \times \int \frac{d^3p}{(2\pi)^3} \frac{d\omega}{(2\pi)}\ \omega\ \gamma_{q,g}(T,\mu_q,p) \rho_f(\omega)\ f_{q,g}(\omega,T,\mu_q)\ \Theta(P^2), \quad \text{(V.3)}$$

where

$$n^{\rm off}_{f,g}(T,\mu_q) = \int \frac{d^3p}{(2\pi)^3} \frac{d\omega}{(2\pi)}\ \omega\ \rho_f(\omega)\ f_{f,g}(\omega,T,\mu_q)\ \Theta(P^2)$$

denotes the off-shell density of quarks, antiquarks or gluons. We note in passing that the shear viscosity η can also be computed using the stress-energy tensor and the Green-Kubo formalism [25]. However, explicit comparisons of both methods in Ref. [25] have shown that the solutions are rather close. This holds especially for the case of the scattering of massive partons where the transport cross section is not very different from the total cross section as also pointed out in Ref. [44].

We show the DQPM* results for η/s, where s is the DQPM* entropy density, in Fig.4 (a) as a function of the temperature. The (upper) orange solid line represents the case of the standard DQPM where the parton masses and widths are independent of momenta as calculated in Ref. [27]. The thick red solid line displays the result obtained in this study using Eqs.(V.1) and (V.2), where the parton masses and width are temperature, chemical potential and momentum dependent. Finally, the black solid line refers to the calculation of η/s in Yang-Mills theory from the Kubo formula using an exact diagrammatic representation in terms of full propagators and vertices from Ref. [45].

Fig. 4 (a) shows that η/s from DQPM* is in the range of the lQCD data and significantly lower than the pQCD limit. As a function of temperature η/s shows a minimum around T_c, similar to atomic and molecular systems [46] and then increases slowly

for higher temperatures. This behavior is very much the same as in the standard DQPM (upper orange line) as shown in Ref. [25]. Therefore, the produced QGP shows features of a strongly interacting fluid unlike a weakly interacting parton gas as had been expected from perturbative QCD (pQCD). The minimum of η/s at $T_c = 158$ MeV is close to the lower bound of a perfect fluid with $\eta/s = 1/(4\pi)$ [47, 48] for infinitely coupled supersymmetric Yang-Mills gauge theory (based on the AdS/CFT duality conjecture). This suggests the "hot QCD matter" to be the "most perfect fluid" [46]. Furthermore, the ratio η/s in DQPM* is slightly larger than in the pure gluonic system (solid black line) due to a lower interaction rate of quarks relative to gluons.

The explicit dependencies of η/s on T and μ_q are shown in Fig.4 (b) where η/s is seen to increase smoothly for finite but small μ_q. We point out again that extrapolations to larger μ_q become increasingly uncertain.

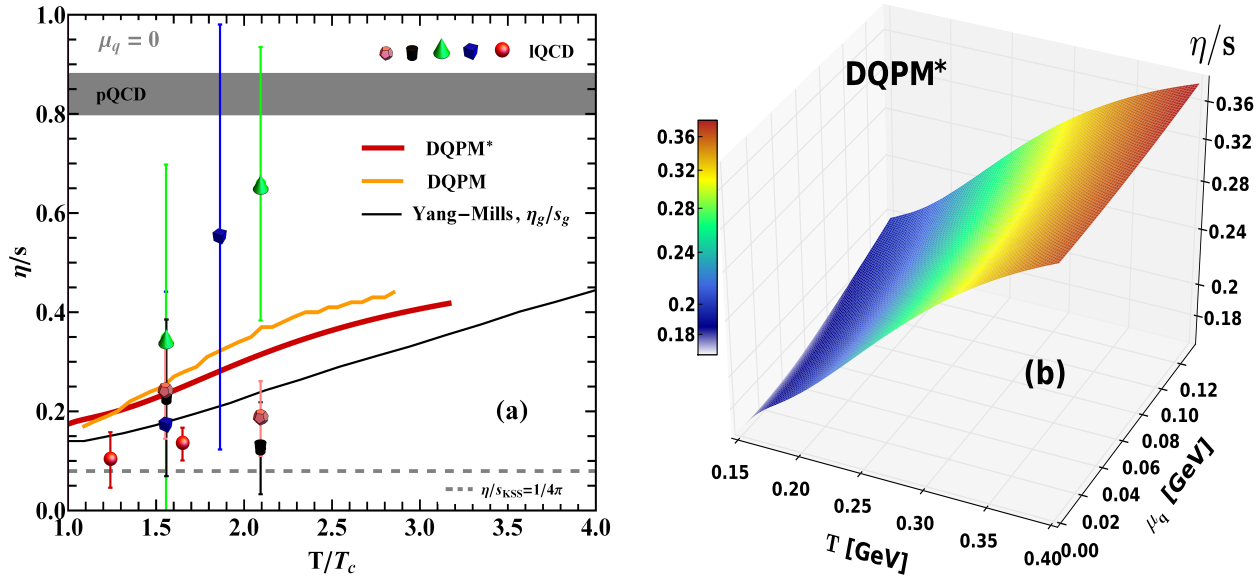

FIG. 4. *(Color online) The shear viscosity to entropy density ratio η/s from different models as a function of temperature T for $\mu_q = 0$ (a) and η/s given by the pDQPM* approach as a function of (T,μ_q) (b). The orange solid line in (a) results from the standard DQPM where the parton masses and widths are independent of momenta [27]. The thick red solid line shows the DQPM* result using Eqs.(V.1) and (V.2), where the parton masses and width are temperature, chemical potential and momentum dependent. The lattice QCD data for pure $SU(3)$ gauge theory are taken from Ref. [49] (red spheres), from Ref. [50] (green pyramid and blue cubic), and from Ref. [51] (black cylinder and pink pynthagone). The orange dashed line gives the Kovtun-Son-Starinets lower bound [47, 48] $(\eta/s)_{KSS} = 1/(4\pi)$. Finally, the black solid line refers to the calculation of η/s in Yang-Mills theory from Ref. [45].*

VI. ELECTRIC CONDUCTIVITY OF THE QGP FROM DQPM*

Whereas the shear viscosity η depends on the properties of quarks and gluons the electric conductivity σ_e only depends on quarks and antiquarks and thus provides independent information on the response of the QGP to external electric fields [52, 53]. The electric conductivity σ_e is also important for the creation of electromagnetic fields in ultra-relativistic nucleus-nucleus collisions from partonic degrees-of-freedom, since σ_e specifies the imaginary part of the electromagnetic (retarded) propagator and leads to an exponential decay of the propagator in time $\sim \exp(-\sigma_e(t-t'))$. Furthermore, σ_e also controls the photon spectrum in the long wavelength limit [54].

We repeat here our previous studies on the electric conductivity $\sigma_e(T)$ [39, 52, 53] for 'infinite parton matter' within the DQPM* using the novel parametrizations of the dynamical degrees of freedom. We recall that the dimensionless ratio σ_e/T in the quasiparticle approach is given by the relativistic Drude formula,

$$\sigma_e(T,\mu_q) = \sum_{f,\bar{f}}^{u,d,s} \frac{e_f^2\, n_f^{\rm off}(T,\mu_q)}{\bar{\omega}_f(T,\mu_q)\ \bar{\gamma}_f(T,\mu_q)},$$

$$\text{with: } \bar{\omega}_f(T,\mu_q) = \left(n_f^{\rm off}(T,\mu_q)\right)^{-1} \times \int \frac{d^3p}{(2\pi)^3}\,\frac{d\omega}{(2\pi)}\ \omega^2\ \rho_f(\omega,\boldsymbol{p})\ f_f((\omega\pm\mu_q)/T), \tag{VI.1}$$

where the quantity $\bar{\omega}_q(T,\mu_q)$ is the quark (antiquark) energy averaged over the equilibrium distributions at finite T and μ_q while $\bar{\gamma}_q(T,\mu_q)$ is the averaged quark width, as given in (V.3).

The actual results for σ_e/T are displayed in Fig.5 (a) in terms of the thick red solid line in comparison to recent lQCD data from Refs. [55–61] and the result from our previous studies within the DQPM [39] (thin orange line). Again we find a minimum in the partonic phase close to T_c and a rise with the temperature T. The explicit dependencies of σ_e/T on T and μ_q, shown in Fig.5 (b), is also increasing smoothly for finite but small μ_q. We finally note that the lower values for σ_e/T in the DQPM* relative to the DQPM result from using the relativistic Drude formula (VI.1) instead of its nonrelativistic counterpart.

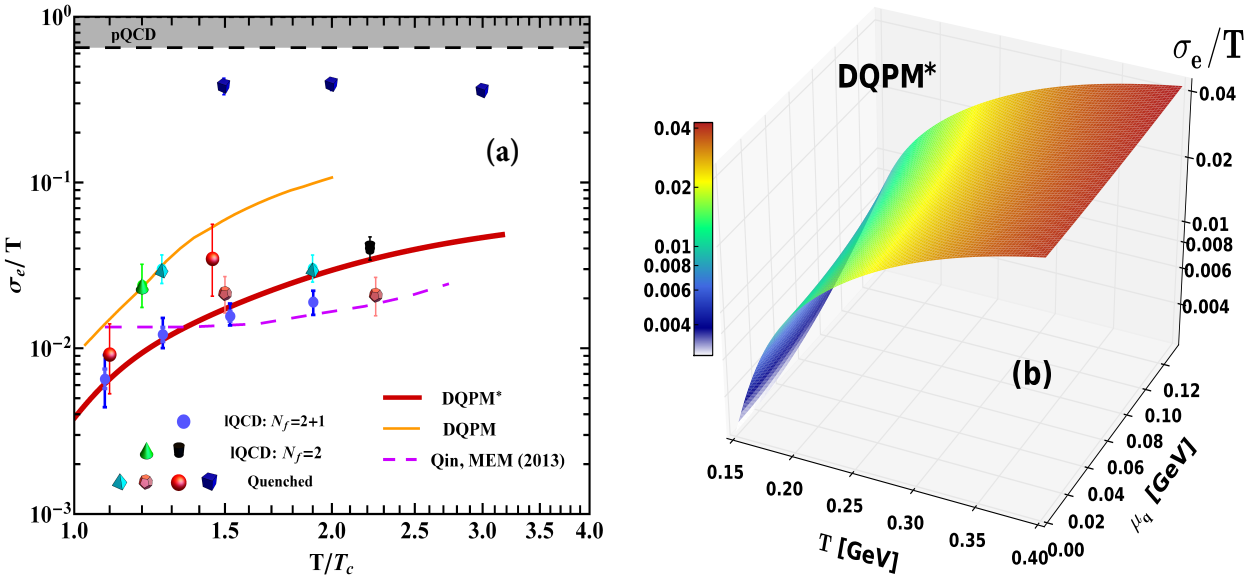

FIG. 5. *(Color online)* σ_e/T *following different models as a function of temperature* T *for* $\mu_q = 0$ *(a) and* σ_e/T *given by the DQPM* approach as a function of* (T,μ_q) *(b). The orange thin solid line in (a) results from the standard DQPM where the parton masses and widths are independent of momenta [27]. The red thick solid line shows the DQPM* result using Eqs.(VI.1), where the parton masses and width are temperature, chemical potential and momentum dependent. The lattice QCD data are taken from Ref. [55] (red spheres), Ref. [56] (pink pentagon), Ref. [57] (blue cubic), Ref. [58] (Cyan pyramid), Ref. [59] (green cone), Ref. [60] (black cylinder), Ref. [61] (blue disk). Qin, MEM (2013) refers to Ref. [62] where a Dyson-Schwinger approach is used. The electric charge is explicitly multiplied out using* $e^2 = 4\pi/137$. *The average charge squared is* $C_{EM} = 8\pi\alpha/3$ *with* $\alpha = 1/137$. *Note that the pQCD result at leading order beyond the leading log [63] is* $\sigma_e/T \approx 5.97/e^2 \approx 65$.

VII. SUMMARY

We have presented in this work an extension of the dynamical quasiparticle model (DQPM) with respect to momentum-dependent selfenergies in the parton propagators which are reflected in momentum-dependent masses and widths. Accordingly, the QGP effective degrees of freedom appear as interacting off-shell quasi-particles with masses and widths that depend on momentum p, temperature T and chemical potential μ_q as given in Eqs. (II.3). These expressions provide a proper high temperature limit as in the HTL approximation and approach the pQCD limit for large momenta p. As in the standard DQPM the effective coupling is enhanced in the region close to T_c which leads to an increase of the parton masses roughly below 1.2 T_c (cf. Fig. 1 a)). Instead of displaying the parton masses as a function of temperature we may alternatively display them as a function of the scalar parton density ρ_s (cf. Ref. [23]) and interpret the masses as a scalar mean-field depending on ρ_s. Since ρ_s is a monotonically increasing function with temperature the masses $M_j(\rho_s)$ will show a minimum in ρ_s for $\rho_s \approx 0.5$ fm^{-3} which specifies the parton density where the effective interaction – defined by the derivative of the masses with respect to the scalar density – changes sign, i.e. the net repulsive interaction at high scalar density becomes attractive at low scalar density and ultimately leads to bound states of the constituents (cf. Ref. [38]).

The extended dynamical quasiparticle model is denoted by DQPM* and reproduces quite well the lQCD results, i.e. the QGP equation of state, the baryon density n_B and the quark susceptibility χ_q at finite temperature T and quark chemical potential μ_q which had been a challenge for quasiparticle models so far [16] (see also Fig. 3b). A detailed comparison between the available lattice data and DQPM* results indicates a very good agreement for temperatures above $\sim 1.2\ T_c$ in the pure partonic phase and therefore validates our description of the QGP thermodynamic properties. For temperatures in the vicinity of T_c (and μ_B= 400 MeV) we cannot expect our model to work so well since here hadronic degrees of freedom mix in a crossover phase which are discarded in the DQPM*.

Furthermore, we have computed also the QGP shear viscosity η and electric conductivity σ_e at finite temperature and chemical potential in order to probe some transport properties of the medium. The relaxation times at finite temperature and chemical potential, used in our study, are evaluated for the dynamical quasi-particles using the parton width which is averaged over the thermal ensemble at fixed T and μ_q. We, furthermore, emphasize the importance of nonperturbative effects near T_c to achieve a small η/s as supported by different phenomenological studies and indirect experimental observations. When comparing our results for η/s to those from the standard DQPM in Ref. [25] we find a close agreement. In the DQPM* the gluon mass is slightly higher (for low momenta) and the quark mass is slightly smaller than in the DQPM. Furthermore, the interaction widths are slightly larger in the DQPM* which finally leads to a slightly lower shear viscosity η than in the DQPM. This also holds for the electric conductivity σ_e which in the DQPM* gives results even closer to the present lQCD 'data'.

In view of our results on the description of QGP thermodynamics and transport properties, one can conclude that the DQPM* provides a promising approach to study the QGP in equilibrium at finite temperature T and chemical potential μ_q. Moreover, we have demonstrated, for the first time, that one can simultaneously reproduce the lQCD pressure and quark susceptibility using a dynamical quasi-particle picture for the QGP effective degrees of freedom. An implementation of the DQPM* in the PHSD transport approach [23] is straight forward and will allow for the description of heavy-ion collisions also for invariant energies $\sqrt{s_{NN}} \approx$ 5-10 GeV.

VIII. ACKNOWLEDGMENT

This work has been supported by the "HIC for FAIR" framework of the "LOEWE" program. The computational resources have been provided by the LOEWE-CSC. Furthermore, the authors acknowledge valuable discussions with R. Marty, P.B. Gossiaux, J. Aichelin, P. Moreau and E. Seifert.

[1] S. Borsanyi, Z. Fodor, C. Hoelbling, S. D. Katz, S. Krieg, C. Ratti, and K. K. Szabo, *Proceedings, 32nd International Symposium on Lattice Field Theory (Lattice 2014)*, PoS **LATTICE2014**, 224 (2015).
[2] S. Borsanyi, Z. Fodor, C. Hoelbling, S. D. Katz, S. Krieg, *et al.*, Phys.Lett. **B730**, 99 (2014).
[3] S. Borsanyi, Z. Fodor, C. Hoelbling, S. D. Katz, S. Krieg, and K. K. Szabo, *Proceedings, 31st International Symposium on Lattice Field Theory (Lattice 2013)*, PoS **LATTICE2013**, 155 (2014).
[4] S. Borsanyi *et al.* (Wuppertal-Budapest), JHEP **1009**, 073 (2010).
[5] S. Borsanyi, G. Endrodi, Z. Fodor, A. Jakovac, S. D. Katz, *et al.*, JHEP **1011**, 077 (2010).
[6] R. A. Soltz, C. DeTar, F. Karsch, S. Mukherjee, and P. Vranas, (2015), 10.1146/annurev-nucl-102014-022157.
[7] S. Borsanyi, G. Endrodi, Z. Fodor, S. Katz, S. Krieg, *et al.*, JHEP **1208**, 053 (2012).
[8] G. Endrodi, Z. Fodor, S. D. Katz, and K. K. Szabo, JHEP **04**, 001 (2011).
[9] M. I. Gorenstein and S.-N. Yang, Phys. Rev. **D52**, 5206 (1995).
[10] P. Levai and U. W. Heinz, Phys. Rev. **C57**, 1879 (1998).
[11] A. Peshier, B. Kämpfer, and G. Soff, Phys. Rev. **C61**, 045203 (2000).
[12] A. Peshier, B. Kampfer, and G. Soff, Phys.Rev. **D66**, 094003 (2002).
[13] V. M. Bannur, Eur. Phys. J. **C50**, 629 (2007).
[14] P. K. Srivastava, S. K. Tiwari, and C. P. Singh, Phys. Rev. **D82**, 014023 (2010).
[15] M. Bluhm, B. Kämpfer, and G. Soff, Phys.Lett. **B620**, 131 (2005).
[16] S. Plumari, W. M. Alberico, V. Greco, and C. Ratti, Phys.Rev. **D84**, 094004 (2011).
[17] A. Bazavov, T. Bhattacharya, M. Cheng, N. Christ, C. DeTar, *et al.*, Phys.Rev. **D80**, 014504 (2009).
[18] E. S. Fraga, A. Kurkela, and A. Vuorinen, Astrophys.J. **781**, L25 (2014).
[19] K. Kajantie, M. Laine, K. Rummukainen, and Y. Schroder, Phys.Rev. **D67**, 105008 (2003).
[20] A. Peshier, Phys.Rev. **D63**, 105004 (2001).
[21] C. Ratti, S. Roessner, and W. Weise, Phys.Lett. **B649**, 57 (2007).
[22] W. Cassing, Eur.Phys.J.ST **168**, 3 (2009).
[23] E. Bratkovskaya, W. Cassing, V. Konchakovski, and O. Linnyk, Nuclear Physics A **856**, 162 (2011).
[24] A. Peshier, J.Phys. **G31**, S371 (2005).
[25] V. Ozvenchuk, O. Linnyk, M. Gorenstein, E. Bratkovskaya, and W. Cassing, Phys.Rev. **C87**, 064903 (2013).
[26] H. Berrehrah, E. Bratkovskaya, W. Cassing, P. Gossiaux, J. Aichelin, *et al.*, Phys.Rev. **C89**, 054901 (2014).
[27] H. Berrehrah, E. Bratkovskaya, W. Cassing, and R. Marty, J.Phys.Conf.Ser. **612**, 012050 (2015).
[28] H. Berrehrah, E. Bratkovskaya, W. Cassing, P. Gossiaux, and J. Aichelin, Phys.Rev. **C91**, 054902 (2015).
[29] A. Peshier and W. Cassing, Phys. Rev. Lett. **94**, 172301 (2005).
[30] G. Aarts and J. M. Martinez Resco, JHEP **02**, 061 (2004).
[31] G. Aarts and J. M. Martinez Resco, JHEP **04**, 053 (2002).
[32] W. Cassing and E. Bratkovskaya, Phys.Rev. **C78**, 034919 (2008).
[33] B. Vanderheyden and G. Baym, J. Stat. Phys. (1998), 10.1023/B:JOSS.0000033166.37520.ae, [J. Statist. Phys.93,843(1998)].

[34] C. S. Fischer, J.Phys. **G32**, R253 (2006).
[35] C. Bonati, M. D'Elia, M. Mariti, M. Mesiti, F. Negro, *et al.*, Phys.Rev. **D90**, 114025 (2014).
[36] L. Rauber and W. Cassing, Phys. Rev. **D89**, 065008 (2014).
[37] W. Cassing and E. Bratkovskaya, Nucl.Phys. **A831**, 215 (2009).
[38] W. Cassing, Nuclear Physics A **791**, 365 (2007).
[39] R. Marty, E. Bratkovskaya, W. Cassing, J. Aichelin, and H. Berrehrah, Phys.Rev. **C88**, 045204 (2013).
[40] J. P. Blaizot, E. Iancu, and A. Rebhan, Phys. Rev. **D63**, 065003 (2001).
[41] C. Allton, S. Ejiri, S. Hands, O. Kaczmarek, F. Karsch, *et al.*, Phys.Rev. **D68**, 014507.
[42] C. Allton, M. Doring, S. Ejiri, S. Hands, O. Kaczmarek, *et al.*, Phys.Rev. **D71**, 054508 (2005).
[43] P. Chakraborty and J. Kapusta, Phys.Rev. **C83**, 014906 (2011).
[44] S. Plumari, A. Puglisi, F. Scardina, and V. Greco, Phys.Rev. **C86**, 054902 (2012).
[45] N. Christiansen, M. Haas, J. M. Pawlowski, and N. Strodthoff, Phys. Rev. Lett. **115**, 112002 (2015).
[46] L. P. Csernai, J. Kapusta, and L. D. McLerran, Phys.Rev.Lett. **97**, 152303 (2006).
[47] G. Policastro, D. T. Son, and A. O. Starinets, Phys.Rev.Lett. **87**, 081601 (2001).
[48] P. Kovtun, D. T. Son, and A. O. Starinets, Phys.Rev.Lett. **94**, 111601 (2005).
[49] H. B. Meyer, Phys.Rev. **D76**, 101701 (2007).
[50] A. Nakamura and S. Sakai, Phys.Rev.Lett. **94**, 072305 (2005).
[51] S. Sakai and A. Nakamura, PoS **LAT2007**, 221 (2007).
[52] W. Cassing, O. Linnyk, T. Steinert, and V. Ozvenchuk, Phys. Rev. Lett. **110**, 182301 (2013).
[53] T. Steinert and W. Cassing, Phys. Rev. **C89**, 035203 (2014).
[54] O. Linnyk, V. Konchakovski, T. Steinert, W. Cassing, and E. L. Bratkovskaya, Phys. Rev. **C92**, 054914 (2015).
[55] H.-T. Ding, A. Francis, O. Kaczmarek, F. Karsch, E. Laermann, *et al.*, Phys.Rev. **D83**, 034504 (2011).
[56] G. Aarts, C. Allton, J. Foley, S. Hands, and S. Kim, Phys.Rev.Lett. **99**, 022002 (2007).
[57] S. Gupta, Phys.Lett. **B597**, 57 (2004).
[58] O. Kaczmarek and M. Müller, PoS **LATTICE2013**, 175 (2014).
[59] B. B. Brandt, A. Francis, H. B. Meyer, and H. Wittig, PoS **ConfinementX**, 186 (2012).
[60] P. Buividovich, M. Chernodub, D. Kharzeev, T. Kalaydzhyan, E. Luschevskaya, *et al.*, Phys.Rev.Lett. **105**, 132001 (2010).
[61] G. Aarts, C. Allton, A. Amato, P. Giudice, S. Hands, *et al.*, JHEP **1502**, 186 (2015).
[62] S.-x. Qin, Phys.Lett. **B742**, 358 (2015).
[63] P. B. Arnold, G. D. Moore, and L. G. Yaffe, JHEP **0305**, 051 (2003).